Modeling a Liquid Crystal Dynamics by Atomistic Simulation with an Ab Initio Derived Force Field

Luca De Gaetani,* Giacomo Prampolini,* and Alessandro Tani*

Dipartimento di Chimica e Chimica Industriale, Università di Pisa, via Risorgimento 35, I-56126 Pisa, Italy

Received: August 3, 2005; In Final Form: December 1, 2005

Atomistic molecular dynamics (MD) simulations of 4-*n*-pentyl 4′-cyano-biphenyl (5CB) have been performed, adopting a specific ab initio derived force field.[1] Two state points in the nematic phase and three in the isotropic phase, as determined in a previous work,[2] have been considered. At each state point, at least 10 ns have been produced, allowing us to accurately calculate single-molecule properties. In the isotropic phase, the values of the translational diffusion coefficient, and even more so the activation energy for the process, agree well with experimental data. Qualitatively, also the dynamic anisotropy of the nematic phase is correctly accounted for. Rotational diffusion coefficients, which describe spinning and tumbling motions, fall well within the range of experimental values. The reorientational dynamics of our model 5CB covers diverse time regimes. The longest one is strongly temperature dependent and characterized by a relaxation time in accord with experimental dielectric relaxation data. Shear viscosity and Landau−de Gennes relaxation times, typically collective variables, reproduce the experimental results very well in the isotropic phase. In the nematic phase, despite a large statistical uncertainty due to the extremely slow relaxation of the correlation functions involved, our simulation yields the correct relative order of the three experimental Miesowicz viscosities.

1. Introduction

Atomistic simulations of complex materials are now becoming more and more feasible,[3−6] despite the computational problems due to the wide range of length and time scales that characterizes their dynamics. As a consequence, increasing attention is being devoted to the construction of potential functions capable of accurately describing the interactions between the material's large molecules.

A possible route to force fields relies on the use of ab initio calculations to sample the potential energy surface (PES) of the dimer. This approach has proven successful for small-to-medium-size molecules (see, e.g., our previous work on benzene and references therein[7]). However, its extension to more complex systems is by no means a straightforward task. This is particularly true for liquid crystals, as typical liquid-crystal forming molecules contain various functional groups, aromatic rings and alkyl chains, with a variety of dispersive, electrostatic, and repulsive contributions to the interaction energy. The latter is also strongly dependent on intramolecular forces and molecular configuration, so that the complex phase behavior of these materials derives from a delicate balance of energetic and entropic effects,[8−11] with an extreme sensitivity of the phase diagram and properties of each (meso)phase to molecular structure details.[8,12]

With the aim of providing efficient force fields to model mesogenic materials,[9,11,13] we have recently developed[14] the fragmentation reconstruction method (FRM) for the construction of intermolecular potentials of large molecules by the use of ab initio information only. Test applications of the FRM have been successful,[1,2,15,16] proving this approach is capable of accurately describing the intermolecular potential energy surface (PES) of a 5CB dimer.[1,14] MD simulations[2] adopting this force field have led to a good agreement with experimental results for the phase diagram, orientational order parameters, and other structural properties of this typical mesogen. In particular, between 290 and 305 K, a kinetically stable, orientationally ordered phase was obtained ($T_m^{exp} = 297.0$ K;[17] $T_{cl}^{exp} = 306.7$[18] − 308[17] K). We consider this result particularly rewarding, as the mesophase was reached starting from three initial configurations with large difference of orientational order parameter. From the methodological point of view, this confirms that runs of at least some 10 ns, as those carried out in ref 2, are required to address the severe ergodicity problems of these systems.

In this work we extend the validation process of the FRM force field to single-molecule and collective dynamic properties. MD results for translational and rotational diffusion coefficients, reorientational (dielectric) relaxation times, and viscosities will be compared to experimental data, in the nematic and isotropic phase close to the nematic transition. Experimental data are more readily available for 5CB than for many other mesogenic materials, making it an ideal test case for force fields. A successful outcome of the validation process would provide some confidence that simulation results of other properties, not easily amenable to experimental determination, for instance, the transverse rotational diffusion coefficient[19−23] or the dielectric relaxation time,[24,25] are also reliable. More importantly, a good agreement with the experiments is vital if one wishes to exploit the huge amount of information available from simulation to intepret the results obtained and, as an ultimate goal, to use simulation for predicting the behavior of materials.

The paper is organized as follows. Section 2 recalls the definitions that are necessary for the following text and gives details of the MD simulations. In the first part of section 3, we present and discuss results relevant to the "fast" dynamics of 5CB, while in the second part the properties that are obtained from slowly relaxing variables, e.g., axis reorientation and viscosities, are discussed. Section 4 collects our main results and conclusions.

* Correspondence to De Gaetani e-mail: degaetani@dcci.unipi.it; Prampolini e-mail: giacomo@dcci.unipi.it; Tani e-mail: tani@dcci.unipi.it

10.1021/jp0542930 CCC: $33.50
Published on Web 01/26/2006

2. Computational Details

All MD simulations were carried out using the force field described in detail in a previous paper.[2] A parallel version of the suitably modified[2] Moscito3.9[26] package was employed.

A system of 192 5CB molecules, for a total of 5184 interaction sites, was equilibrated in the NPT ensemble, with P = 1 atm and different temperatures for ≃40 ns[2]. Temperature and pressure were kept constant using the weak coupling scheme of Berendsen et al.[27] Conversely, production runs were performed in the microcanonical (NVE) ensemble, to leave particle velocities unperturbed.

During all equilibration and production runs, the bond lengths were kept fixed at their equilibrium value using the SHAKE algorithm[28] and a time step of 1 fs was used. The short-range intermolecular interactions have been truncated at $R_c = 10$ Å, employing standard corrections for energy and virial.[29] Charge−charge long-range interactions were treated with the particle mesh Ewald (PME) method,[30,31] using a convergence parameter α of $5.36/2R_c$ and a fourth order spline interpolation.

The dynamical properties of 5CB have been divided in short-time properties, whose correlations decay in the picosecond regime, and long-time properties, whose relaxation requires 10−100 ns. Among the former, translational dynamics in the isotropic phase is conveniently expressed by the diffusion coefficient D, defined either as the long time limit of the center of mass mean square displacement (MSD) or the time integral of the velocity autocorrelation function (acf), i.e.,

$$D = \lim_{t\to\infty} \frac{1}{2t} \mathrm{MSD}(t) = \frac{1}{3}\int_0^\infty \langle v(t)\, v(0)\rangle \, \mathrm{d}t \tag{1}$$

Note that the symbol $\langle\ \rangle$ indicates a double statistical average over all molecules and successive time origins. This notation will be used for all the single-particle properties. For the nematic phase, the longitudinal ($D_{||}$) and transverse ($D_\perp$) diffusion coefficients were computed, by means of eq 1, from the velocities projected onto and perpendicular to the phase director $\hat{\mathbf{n}}$. The latter is obtained as the eigenvector corresponding to the maximum eigenvalue P_2 of the Saupe ordering matrix $\mathbf{Q}$.[32] Moreover, the isotropic (D_{iso}) diffusion coefficient of the nematic phase has been computed using the standard definition

$$D_{iso} = D_{||}^{1/3} D_\perp^{2/3} \tag{2}$$

Rotational motions, i.e., molecular spinning and tumbling, have been studied, in both condensed phases, by computing parallel ($D_{||}^R$) and perpendicular ($D_\perp^R$), rotational diffusion coefficients, respectively. The latter are defined[33] as

$$D_k^R = \int_0^\infty \langle \omega_k(t)\cdot\omega_k(0)\rangle \, \mathrm{d}t;\ k = ||, \perp \tag{3}$$

where $\omega_{||}$ and $\omega_\perp$ are the parallel and perpendicular projections of the molecular angular velocity $\boldsymbol{\omega}$ onto the 5CB para axis ($\hat{\mathbf{u}}$) of the biphenyl moiety.

Conversely, dielectric relaxation and viscosities involve dynamic processes that take place on much longer time scales. The dielectric relaxation function $M(t)$ is usually expressed as the time correlation function of the molecular dipoles $\boldsymbol{\mu}$ ($M(t) = \langle \mu(0)\cdot\mu(t)\rangle$). In the 5CB molecule, however, since the dipole moment, essentially due to the polar CN group, lies along $\hat{\mathbf{u}}$,[2,34,35] the dielectric relaxation time can be computed as the reorientation time (τ_R) of such axes. Molecular reorientation has been studied in both isotropic and nematic phases. In the former, the acf of the $\hat{\mathbf{u}}$ axis has been employed in the calculation of the first and second rank Legendre polynomials C^1 and C^2, i.e.

$$C^1(t) = \langle \hat{\mathbf{u}}(t)\cdot\hat{\mathbf{u}}(0)\rangle \tag{4}$$

$$C^2(t) = \frac{3}{2}\langle (\hat{\mathbf{u}}(t)\cdot\hat{\mathbf{u}}(0))^2\rangle - \frac{1}{2} \tag{5}$$

Conversely, as regards the nematic phase, the projection $u_n(t)$ of $\hat{\mathbf{u}}(t)$ onto $\hat{\mathbf{n}}(0)$ (i.e., the director at time $t = 0$) has been considered in the definitions

$$\Phi_{00}^1(t) = \langle u_n(t) u_n(0)\rangle \tag{6}$$

$$\Phi_{00}^2(t) = \frac{3}{2}\langle [u_n(t) u_n(0)]^2\rangle - \frac{1}{2} \tag{7}$$

The reorientation time τ_R, defined as a time integral, was calculated by fitting both $C^1(t)$ and $\Phi_{00}^1(t)$ with a function $F(t)$

$$F(t) = \sum_{i=1}^{N_{exp}} \mathrm{e}^{-t/\tau_i} \tag{8}$$

as suggested by recent dielectric relaxation measurements performed in the nematic phase.[25]

Finally, activation energies have been estimated by assuming an Arrhenius dependence of the relevant quantities on temperature.

The behavior of some collective dynamic properties has also been computed. In this case, the symbol $\langle\ \rangle$ indicates a statistical average over successive time origins. In the isotropic phase, the shear (η_S), longitudinal (η_L), and bulk (η_B) viscosities were calculated from the time integral of the correlation function of the proper elements of the stress tensor $\hat{\boldsymbol{\sigma}}$.[36]

$$\eta_S = \frac{V}{6k_B T}\int_0^\infty \sum_{\alpha=1}^{3}\sum_{\beta\neq\alpha}^{3} \langle \sigma_{\alpha\beta}(0)\sigma_{\alpha\beta}(t)\rangle \, \mathrm{d}t \tag{9}$$

$$\eta_L = \frac{V}{3k_B T}\int_0^\infty \sum_{\alpha=1}^{3} \langle \sigma_{\alpha\alpha}(0)\sigma_{\alpha\alpha}(t)\rangle \, \mathrm{d}t \tag{10}$$

$$\eta_B = \eta_L - \frac{4}{3}\eta_S = \frac{V}{9k_B T}\int_0^\infty \sum_{\alpha,\beta=1}^{3} \langle \sigma_{\alpha\alpha}(0)\sigma_{\beta\beta}(t)\rangle \, \mathrm{d}t \tag{11}$$

where V is the volume of the simulation box and k_B the Boltzmann constant.

The time integrals have been fitted with the following expression

$$f(t) = a_1(1 - \exp(-a_3 t)) + a_2(1 - \exp(-a_4 t)) \tag{12}$$

and the sum of the amplitudes yields the viscosity.

In the orientationally ordered phase, the fluctuations of the director $\hat{\mathbf{n}}$ (assumed along z) have been monitored through its angular velocity ($\hat{\boldsymbol{\Omega}}$) acf, whose time integral is defined as[37]

$$\Phi_{\Omega\Omega} = \frac{V}{k_B T}\int_0^\infty \mathrm{d}t\, \langle \Omega(t)\Omega(0)\rangle;\ \Omega = \frac{\Omega_x + \Omega_y}{2} \tag{13}$$

Furthermore, we have calculated Miesowicz (η_1^M, η_2^M, η_3^M) and Helfrich (η_{12}^H) viscosities, whose definitions are given in Figure 1 and eq 19.

In the following Green−Kubo expressions,[38] the correlation functions (cf) of the stress tensor elements have been employed

in the definitions of the quantities

$$\eta_{ijkl} = \frac{V}{k_B T}\int_0^\infty \mathrm{d}t\, \langle \sigma_{ij}(t)\sigma_{kl}(0)\rangle \quad (14)$$

$$\eta_{\sigma\Omega} = \frac{V}{k_B T}\int_0^\infty \mathrm{d}t\, \langle \sigma^s_{zx}(t)\Omega_y(0)\rangle = \frac{V}{k_B T}\int_0^\infty \mathrm{d}t\, \langle \sigma^s_{yz}(t)\Omega_x(0)\rangle \quad (15)$$

$$\eta_{\sigma\Omega}{}^* = \frac{V}{k_B T}\int_0^\infty \mathrm{d}t\, \langle \sigma^a_{zx}(t)\Omega_y(0)\rangle = \frac{V}{k_B T}\int_0^\infty \mathrm{d}t\, \langle \sigma^a_{yz}(t)\Omega_x(0)\rangle = \frac{1}{2} \quad (16)$$

where σ^s_{ij} and σ^a_{ij} are, respectively, the elements of the symmetric and antisymmetric pressure tensors, i.e.:

$$\sigma^s_{ij} = \frac{1}{2}[\hat{\boldsymbol{\sigma}}+\hat{\boldsymbol{\sigma}}^\dagger]_{ij} - \frac{1}{3}Tr(\hat{\boldsymbol{\sigma}})\,;\ \sigma^a_{ij} = \frac{1}{2}[\hat{\boldsymbol{\sigma}} - \hat{\boldsymbol{\sigma}}^\dagger]_{ij} \quad (17)$$

The uniaxial phase symmetry was exploited to improve accuracy assuming equivalent the two components tranverse to the director, so that we can define

$$\eta_{\alpha\alpha zz} = \frac{\eta_{xxzz} + \eta_{yyzz}}{2};\ \eta_{\alpha z\alpha z} = \frac{\eta_{xzxz} + \eta_{yzyz}}{2};\ \eta_{\alpha\alpha\alpha\alpha} = \frac{\eta_{xxxx} + \eta_{yyyy}}{2}$$

We also define combinations of the above terms that will be useful in the following:

$$\eta_S = \frac{1}{3}(2\eta_{\alpha z\alpha z} + \eta_{xyxy}) - \frac{2\eta_{\sigma\Omega}\eta_{\Omega\sigma}}{3\Phi_{\Omega\Omega}};\ \tilde{\eta}_1 = 2(\eta_{z\alpha z\alpha} - \eta_{xyxy}) - \frac{2\eta_{\sigma\Omega}\eta_{\Omega\sigma}}{\Phi_{\Omega\Omega}};$$

$$\tilde{\eta}_2 = -\frac{\eta_{\sigma\Omega}}{\Phi_{\Omega\Omega}};\ \tilde{\eta}_3 = \frac{3}{4}(\eta_{zzzz} + 2\eta_{\alpha\alpha\alpha\alpha}) - 2\eta_{z\alpha z\alpha} - \eta_{xyxy} + 2\frac{\eta_{\sigma\Omega}\eta_{\Omega\sigma}}{\Phi_{\Omega\Omega}}$$

Finally, the rotational viscosity coefficient γ_1 can be computed as

$$\gamma_1 = 2\frac{\eta^*_{\sigma\Omega}}{\Phi_{\Omega\Omega}} \quad (18)$$

while the Miesowicz viscosities can be expressed as appropriate combinations of the latter quantities:

$$\eta^M_1 = \eta_S + \frac{\tilde{\eta}_1}{6} + \tilde{\eta}_2 + \frac{\gamma_1}{4};\ \eta^M_2 = \eta_S + \frac{\tilde{\eta}_1}{6} - \tilde{\eta}_2 + \frac{\gamma_1}{4}\,;\ \eta^M_3 = \eta_S - \frac{\tilde{\eta}_1}{3} \quad (19)$$

It is also convenient to consider the quantity

$$\eta^H_{12} = 2\tilde{\eta}_3$$

called the Helfrich viscosity. It may be of some interest to note that in the isotropic phase, the quantities $\tilde{\eta}_1$ and $\tilde{\eta}_2$, as well as γ_1, vanish and the three Miesowicz viscosities become all equal to η_S.

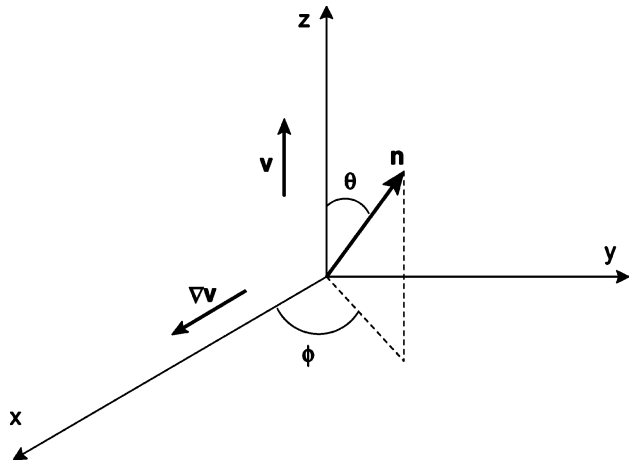

Figure 1. Definition of Miesowicz and Helfrich viscosities. $\hat{\mathbf{n}}$, $\mathbf{v}$, and $\nabla\mathbf{v}$ are the director and the velocity field of the flow and its gradient, respectively. The coefficients η^M_1, η^M_2, η^M_3, and η^H_{12} are obtained considering the following four geometries: η^M_1, $\theta = 0$; η^M_2, $\theta = \pi/2$, $\phi = 0$; η^M_3, $\theta = \pi/2$, $\phi = \pi/2$; η^H_{12}, $\theta = \pi/4$, $\phi = 0$.

Particular attention has been paid to the evaluation of the error in both the functions and the integrals that involve the calculation of collective properties. If Zwanzig's procedure[39] is applied, the error can be evaluated by the function $\Delta c_Z(t)$, defined as

$$\Delta c_Z(t) = \frac{2\tau(t)}{T_{run}} \quad (20)$$

where T_{run} is the length of the run and $\tau(t)$ the correlation time of the appropriate cf. $c(s)$, i.e.,

$$\tau(t) = 2\int_0^t \mathrm{d}s\, c(s)$$

Equation 20 is based on the assumption of Gaussian behavior of variables and might lead to unphysical conclusions.

As an alternative approach to error evaluation, we define a slightly modified version of eq 20:

$$\Delta c(t) = \frac{2\tau(t)}{T_{run}} c(t) \quad (21)$$

This equation implies that the error will vanish in the long time limit, where $c(t)$ goes to zero. At each time t we can now consider the function $c(t) \pm \Delta c(t)$, where the $\pm$ defines $c_{MAX}(t)$ and $c_{MIN}(t)$, respectively. The integrals of these two functions (MAX and MIN) represent the upper and lower bound of the integral of $c(t)$.

3. Results and Discussion

3.1. Short Time Properties. A system of 192 5CB molecules was prepared in its experimental crystalline structure[40] and equilibrated at 250 K at atmospheric pressure. Several runs of ≃40 ns were then performed at increasing temperatures, so to observe stable crystalline (T < 280 K), nematic (290 K < T < 305 K), and isotropic (T > 305 K) phases. Such procedure and the resulting thermodynamic quantities have been described in detail in a previous paper.[2] After equilibration, five different runs at selected temperatures, namely 290, 300, 310, 315, and 330 K, were extended in the NPT ensemble for an additional ≃3 ns. From these runs, two configurations were extracted after 1 and 3 ns of simulation and used as starting points for sets of

TABLE 1: Thermodynamic Quantities Averaged on Different Runs

runs	t_{run} (ns)[a]	T (K)	ρ (g/cm^3)	P_2	P_4
⟨1,2,3⟩	28	290 ± 3	1.086	0.55 ± 0.05	0.24 ± 0.02
⟨4,5⟩	15	300 ± 3	1.073	0.42 ± 0.02	0.11 ± 0.02
⟨6,7⟩	20	310 ± 3	1.059	0.20 ± 0.03	0.06 ± 0.03
⟨8,9⟩	10	315 ± 3	1.055	0.15 ± 0.02	0.04 ± 0.03
⟨10,11⟩	10	330 ± 3	1.051	0.12 ± 0.01	0.01 ± 0.01

[a] Total simulation time of the MD-NVE runs.

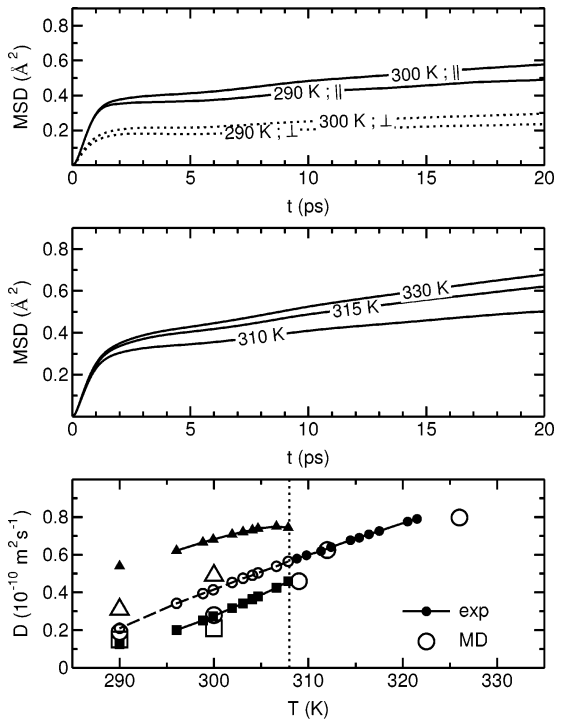

Figure 2. MSD values as a function of T for the nematic (upper panel) and isotropic (middle panel) phase. In the nematic phase (290 and 300 K), MSD is shown in parallel (full line) and perpendicular (dotted line) direction with respect to the director. In the lower panel the computed translational diffusion coefficients (open symbols) are compared with the experimental NMR measures[41] (filled symbols and lines). In the isotropic phase ($T \geq 310$ K), all experimental and computed data are reported as circles, while in the ordered phase, $D_{\parallel}$, $D_{\perp}$, and D_{iso} are reported as triangles, squares, and circles, respectively. Note that the experimental values at 290 K were extrapolated assuming an Arrhenius temperature dependence of the relevant D_k. Experimental clearing temperature ($T_{cl}^{exp} = 308$ K) is reported as a vertical dotted line.

NVE-MD runs, totaling production runs of at least 10 ns at each temperature. The resulting temperatures, densities, and order parameters have been averaged on the runs and are reported in Table 1.

Translational Diffusion. The center of mass MSD, computed at each temperature, is reported in Figure 2. In the nematic phase at 290 and 300 K (upper panel), one can see a marked difference between the longitudinal and transverse components of the MSD functions. No major difference is observed among the MSD x, y, and z components at higher temperatures. From the velocity acf values, translational diffusion coefficients were computed following eq 1 and are reported as a function of temperature in the lower panel of Figure 2, while the computed D values, averaged on the two sets of run for each temperature, are compared with their experimental values[41] in Table 2. The activation energy estimated from all values, including D_{iso} of the nematic phase, is 32.3 ± 5 kJ/mol in very good agreement with the experimental result 32.8 ± 0.5 kJ/mol.[41] Although this accord might well be fortuitous, it is certainly rewarding as

TABLE 2: Computed (D_k) and Experimental[41] (D_k^{exp}) Translational Diffusion Coefficients in Nematic and Isotropic Phase[a]

T (K)	D_k (× 10^{-10} m^2/s)	D_k^{exp} (× 10^{-10} m^2/s)
290 (k = ∥)	0.31	0.54
290 (k = ⊥)	0.15	0.13
290 (k = iso)	0.19	0.21
300 (k = ∥)	0.49	0.66
300 (k = ⊥)	0.21	0.27
300 (k = iso)	0.28	0.37
310 (k = iso)	0.46	0.60
315 (k = iso)	0.63	0.69
330 (k = iso)	0.80	0.93

[a] The experimental value at 290 K was obtained by assuming an Arrhenius temperature dependence of the measured quantities.

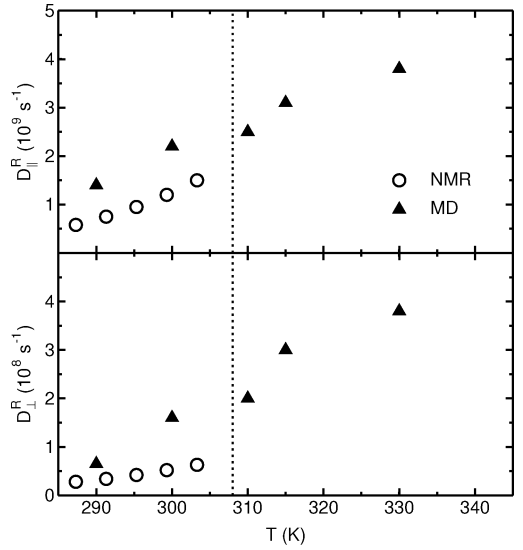

Figure 3. Longitudinal ($D_{\parallel}^R$) and transverse ($D_{\perp}^R$) rotational diffusion coefficients. Experimental[21] (circles) and computed (triangles) values are reported as a function of temperature T.

activation energies are considered among the most reliable experimental data.

From these data it appears that the translational diffusion is well reproduced in the isotropic phase. Close to the transition to the nematic phase, a small residual amount of orientational order is present ($P_2 \simeq 0.2$), probably due to the relatively small number of molecules in the system. The latter residual order might be the cause of the worse agreement of the D coefficient with its experimental value at 310 K. As regards the nematic phase, parallel and transverse diffusion coefficients are clearly resolved (see triangles and squares in the bottom panel of Figure 2), though less than experimental values. D_{iso}, computed as reported in eq 2, is in quite satisfactory agreement with the extrapolated experimental data[41] at 290 K, but less at 300 K.

Rotational Diffusion. The molecular spinning and tumbling have been monitored through the $D_{\parallel}^{rot}$ and $D_{\perp}^{rot}$ diffusion coefficients, respectively (see eq 3). These are compared in Figure 3 with the relevant experimental values, obtained by NMR measurements[19−21] in the nematic phase. The experimental data of $D_{\perp}^{rot}$ in nematic bulk phases seem to suffer of a certain degree of indeterminacy,[22,23] so that they are often biased by some model approximation[21] or assumed.[19,20] The literature values of $D_{\parallel}^{rot}$, reported for 5CB,[19−21] range from 0.5 to 3.5 × 10^9 s^{-1}, which well agree with our computed values of 1.4 × 10^9 s^{-1} and 2.2 × 10^9 s^{-1} at 290 and 300 K, respectively. Considering this good accord with the parallel coefficient, MD

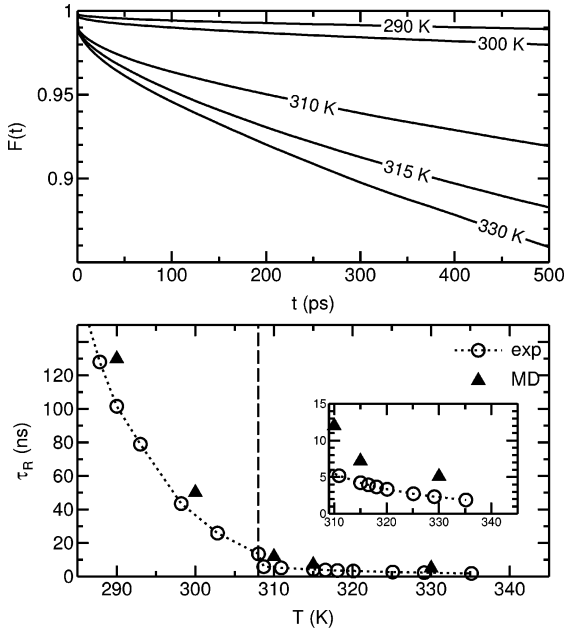

Figure 4. Dielectric relaxation functions $F(t)$ and dielectric relaxation times (τ_R). In the upper panel the computed functions $F(t) = \Phi^1{}_{00}(t)$ and $F(t) = C^1(t)$, defined in eqs 6 and 4, are shown for the nematic (T = 290 K, T = 300 K) and the isotropic (T = 310, 315, and 330 K) phases, respectively. The experimental[25,42] (circles) and computed (black triangles) relaxation times (τ_R) are reported in the lower panel as a function of temperature T. The temperature dependence in the isotropic phase is detailed in the inset of the lower panel.

TABLE 3: Computed (τ_R) and Experimental (τ_R^{exp}) Dielectric Relaxation Times in the Isotropic[42] and Nematic[25] Phases[a]

T (K)	τ_R^{exp} (ns)	τ_R (ns)	τ_1 (ns)	τ_2 (ps)	τ_3 (ps)	τ_4 (ps)
290	101.6	130 ± 35	130	208 ± 53	18 ± 2.3	0.5 ± 0.01
300	35.3	51 ± 26	51	153 ± 54	18 ± 3	0.5 ± 0.02
310	5.2	12 ± 3.8	11.8	210 ± 42	26 ± 4	0.5 ± 0.02
315	4.2	7.2 ± 2.1	7.0	200 ± 29	20 ± 3	0.5 ± 0.01
330	2.3	5.3 ± 1.8	5.1	170 ± 26	15 ± 2	0.5 ± 0.01

[a] In the last four columns, the fitting parameters τ_i for the long axis reorientational acf (see eq 8) are given. The reported uncertainties have been obtained from the independent runs shown in Table 1.

simulations may be considered an additional technique to possibly overcome the indeterminacy on $D_\perp^{rot}$.

3.2. Long Time Properties. The rheodielectric behavior of 5CB has been studied by monitoring the long axis reorientation as well as the viscosities in the bulk. Both these phenomena involve dynamic processes that take place on a much longer time scale than that underlying diffusion. Therefore, the simulations have been extended as long as possible (≃10 ns in the isotropic phase and ≥15 ns in the nematic) to improve the statistical accuracy.

Dielectric Relaxation. From the upper panel of Figure 4, where the reorientational correlation function ($F(t)$) is reported for each temperature, it is evident that the relaxation process occurs on the ns time scale, being $F(t)$ reduced, after 0.5 ns, by <20% in the isotropic phase and by <5% in the ordered phase. The marked difference can be attributed to the effect of the nematic mean field, which constrains the molecular long axis to tumble around a preferred orientation aligned with the director, thus reducing the relaxation rate.

All computed dielectric relaxation times are reported in Table 3 together with their experimental values for both isotropic[42] and nematic[25] phases. We are not using the collective dipole correlation function for the comparison with dielectric relaxation measurements, as the statistical uncertainty of the MD results is too large to provide reliable data. However, the difference between collective and individual relaxation times is not expected to be dramatic for 5CB.

TABLE 4: Computed and Experimental[46] Values of the Shear (η_S) and Longitudinal Viscosity (η_L) in the Isotropic Phase[a]

T (K)	η_S (mPa s)	η_L (mPa s)	η_S^{exp} (mPa s)
310	25.4 ± 7	94	23.8
315	22.2 ± 6	75	19.0
330	12.0 ± 3	33	11.0

[a] The reported standard deviation has been obtained averaging over different off-diagonal components and runs.

The τ_R temperature dependence in the isotropic phase is studied in ref 42 for 4CB and 5CB. The former, which does not possess LC phases, shows an Arrhenius type dependence, while 5CB exhibits strong deviations approaching the transition. Although overestimating the experimental values, our model well reproduces this non-Arrhenius behavior, as shown in the inset of Figure 4. Furthermore, the higher relaxation times in the isotropic phase at 310 K could be explained, as for the diffusion coefficients, by considering the residual order still present ($<P_2> \simeq 0.2$) near the transition.

In the last four columns of Table 3, the fitted times entering eq 8 τ_i (i = 1,4) are reported. It is apparent that their accuracy worsens for the slowest process, which takes place on a ns time scale, due to the limited, though computationally long, time of our runs. However, it is also apparent that the increase by almost 2 orders of magnitude of the relaxation times in the transition from isotropic to nematic phase is correctly accounted for by our results.

The widely different values clearly indicate rather diverse dynamic regimes. The longest one, which is strongly temperature dependent, might involve the coherent motion of group of molecules, while the fastest is essentially temperature independent and probably related to intramolecular rearrangements, that may influence the long axis definition and, therefore, the molecular dipole. In particular, the ultrafast τ_4 time well reproduces the experimental optical Kerr effect (OKE) value.[43] Also, the temperature dependence of our computed τ_i values correctly reproduces the experimental findings.[43−45]

Isotropic Viscosities. As can be seen from the data reported in Table 4, the agreement between experimental[46] and computed shear viscosities is very good at all temperatures. From these values, following Landau−de Gennes (LdG) theory,[8] the relaxation time (τ_{LdG}), which is related to the randomization process of the pseudo-nematic domains,[8,44] can be computed as

$$\tau_{LdG} = \frac{V^*_{eff}\,\eta_S(T)}{k_B(T - T^*)} \qquad (22)$$

where V^*_{eff} has been taken as the simulation box volume divided by the number of molecules, k_B is the Boltzmann constant, and we have used for T^* the nematic-to-isotropic transition temperature (T_{NI} = 305 K).

The agreement between computed τ_{LdG} values and experimental OKE results (τ_{LdG}^{exp} (ref 43)) derives from the aforementioned good description of viscosity, assuming a similar estimate of the effective molecular volume V^*_{eff}.

Nematic Viscosities. The computation of viscosities via Green−Kubo relations requires long runs because of the collective nature of the dynamics involved. In the present case the problem is made more severe by the long time tails of the

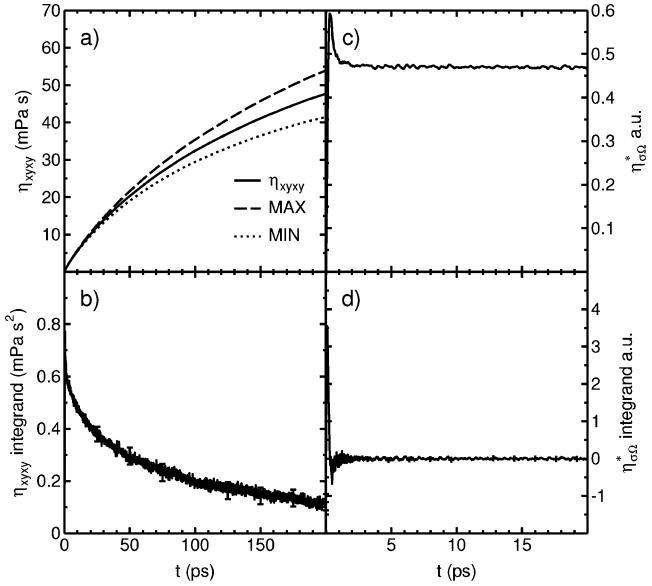

Figure 5. Fast and slowly converging cf values with their integral, required to evaluate viscosities in the nematic phase. (a) η_{xyxy} and the maximized (MAX, dashed) and minimized (MIN, dotted) functions defined in section 2. (b) Integrand function of η_{xyxy} (see eq 14). The error (black bars) has been computed as described in the computational details section. (c) Convergence of $\eta_{\sigma\Omega}$* to the predicted theoretical value of 0.5. (d) Integrand of $\eta_{\sigma\Omega}$*. Note the much smaller error bars, due to the faster decay of the cf.

correlation functions of the stress tensor components (see eq 14−19)). As a consequence, the nematic viscosities were computed only at 290 K, where we performed a production run of about 28 ns saving the stress tensor data each 2 fs. Unlike the isotropic phase, where we can choose every coordinate system as a reference frame, the lower symmetry of the nematic phase leads to equations 19, which do depend on the reference system and hold in a fixed director frame.[47] We actually did not constrain the director, but satisfied the condition of a fixed director frame as in ref 37, i.e. rotating the stress tensor at each step to align the director to the *z*-axis.

We can distinguish two sets of viscosities: slowly converging integrals (η_{ijkl}, see eq 14) evaluated up to 200 ps and faster integrals (see eqs 13, 15, and 16) well converged within 20 ps. An example of the former group is shown in panel (a) of Figure 5, while panel (c) reports the much faster $\eta_{\sigma\Omega}$*, whose value 0.471 ± 0.005 agrees satisfactorily with the theoretical prediction of 0.5. The $\hat{\Omega}$ acf also loses its memory very quickly, so that its integral $\Phi_{\Omega\Omega}$ reaches its asymptotic value after 5 ps (see Figure 6), although the director's dynamics is very slow, even for a small system as ours. This means that the director is moving with fast vibrational motions around its mean direction which varies on a time scale of only two or three orders of magnitude longer.

The integrals of the cf with the long time tail, and the corresponding MIN and MAX functions, did not converge in the 200 ps time window, hence we fitted them with a two-exponential function:

$$I(t) = a_1(1 - \exp(-t/\tau_1)) + a_2(1 - \exp(-t/\tau_2)) \quad (23)$$

taking $a_1 + a_2$ as the integral value.

The Miesowicz viscosities have been evaluated according to the definition given in eq 19. The comparison with experimental data obtained by a slot viscosimeter[48] and dynamic light scattering,[49] reported in Table 6, is encouraging. Despite large errors, the computed data reproduce the correct experimental

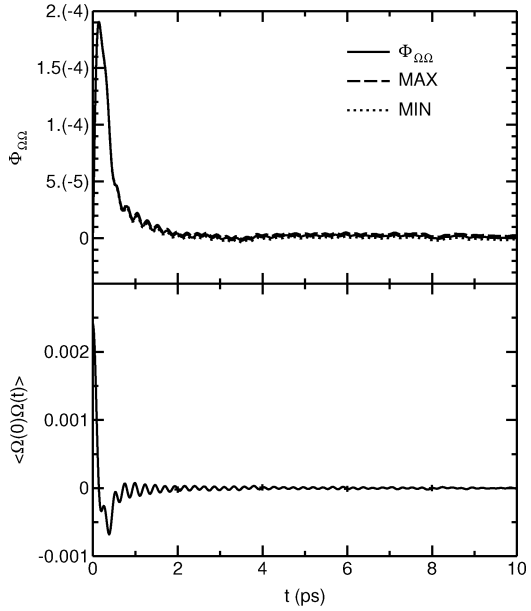

Figure 6. Director angular velocity acf and its integral $\Phi_{\Omega\Omega}$. Due to the small error (black bars in the lower panel) on the acf, $\Phi_{\Omega\Omega}$ and its MAX and MIN functions (defined in section 2) are almost indistinguishable in the upper panel.

TABLE 5: Computed and Experimental[43] Values of the Landau−De Gennes Relaxation Times in the Isotropic Phase

T (K)	τ_{LdG}(ns)	τ^{exp}_{LdG} (ns)
310	144	139
315	63	49
330	11	9

TABLE 6: Computed and Experimental Miesowicz Viscosities[48,49] and Rotational Viscosity Coefficient[50,51] γ_1

	η_1^M (mPa s)	η_2^M (mPa s)	η_3^M (mPa s)	γ_1 (mPa s)
MD[a]	51 ± 19	118 ± 19	59 ± 22	44 ± 14
exp	25−22	130−117	50−42	100−120

[a] Errors on the MD values are computed according to eq 21 and following text.

trend,[8,48,49] $\eta_2^M > \eta_3^M > \eta_1^M$ that is due to the relative difficulty of the director motion when subject to different shear strains.

There are several methods to evaluate the rotational viscosity coefficient γ_1, e.g., a statistical approach[52] or nonequilibrium atomistic MD methods.[53] For instance, the 5CB γ_1 value has been computed recently[54] by applying the aforementioned statistical approach[52] to MD runs of $\simeq$1 ns, performed on a system of 64 molecules. In the following we adopt the direct approach of Sarman and Evans.[38] The resulting γ_1, reported in Table 3, agrees with those computed in ref 54, within the experimental error. Conversely, the large underestimation of the experimental data might be due to the small size of our system. As shown in ref 37, when the system dimensions increase, the director displacement and $\Phi_{\Omega\Omega}$ decrease, which leads to higher values of γ_1 (see eq 18). We expect that our result for γ_1 is correct for the system studied and that it might approach experimental value with a larger number of molecules.

Despite the low value for γ_1, η_2^M and η_3^M are very close to experimental data: this agreement might be the result of an overestimated η_{ijkl} that compensates the underestimated γ_1.

4. Conclusions

In this paper we have completed the process of validation of a new force field, specifically designed to model interactions

between 5CB molecules.[1,2] This force field has already given satisfactory results for static properties.[2] Among them, we stress a good reproduction of the phase diagram of this material, with an orientationally ordered phase that is stable between ≃290 and ≃305 K, over a simulation time of some 10 ns. Though this is no proof of thermodynamic stability of the phase, we could reach the same average value of P_2 (≃0.54 at 290 K) starting from three configurations with P_2 ranging from 0.46 to 0.75. As for the alkyl chain, the description of the shift of the distribution of conformers that accompanies the isotropic to nematic transition also agrees well with the data extracted from NMR measurements,[55] showing a significant increase of the population of more extended conformers in the nematic phase.

In the present paper we test the performance of the new force field by comparing simulated and experimental results for an array of single-molecule and collective dynamic properties.

Translational diffusion appears to be well described over the whole temperature range we explored. In the nematic phase, the anisotropy of the center of mass motion is correctly accounted for, although the simulated $D_{\parallel}$ and $D_{\perp}$ are less separated than their experimental counterparts. On the other hand, their average value is in almost quantitative agreement with the (extrapolated) experimental data at 290 K, less at 300 K. In the isotropic phase the reproduction of experimental data is quite satisfactory at 315 K, but less accurate at 310 and 330 K. However, the MD estimate of the activation energy agrees very well with the measured one.

It is less easy to assess the quality of modeling of the rotational motion, as the experimental data are rather scattered, with $D_{\perp}^{\mathrm{rot}}$ ranging from 0.1 to 0.7 10^8 s^{-1} in the nematic phase.[19−21] However, our results are well within the range of measured values for both $D_{\parallel}^{\mathrm{rot}}$ and $D_{\perp}^{\mathrm{rot}}$.

The overall good representation of single-molecule dynamics is a basis for confidence that collective dynamic properties also might be within the scope of our model.

Actually, shear viscosity data as well as Landau−de Gennes relaxation times agree very well with measured values in the isotropic phase. In the nematic phase, our estimate of Miesowicz viscosities is qualitatively correct for η_2 and η_3, but largely in excess of the experimental data for η_1, while the opposite defect is found for the rotational viscosity coefficient γ_1. It must be noted that the very slow dynamics of the system at 290 K and the collective nature of these properties lead to significant statistical uncertainty on the MD results, despite an almost 30 ns long run. Hence, it would be premature to draw definite conclusions on the quality of our modeling of collective dynamics in the nematic phase.

From the summary above, we can conclude that our model provides a satisfactory description of many structural and dynamic properties of a typical liquid crystal as 5CB. This is obviously a necessary condition to be fulfilled before exploiting the large amount of detailed information contained in the MD trajectories to gain insights into the microscopic processes underlying the observed results. For instance, we plan to assess the role of the alkyl chain dynamics and conformer distribution changes in the isotropic to nematic transition, as this is likely a key step of the ordering process in these materials. Tumbling motion and its relation with reorientational dynamics also deserve a closer inspection, both for its connection with the rotational viscosity coefficient, an important feature for technological applications, and for the difficulties still present in its experimental determination.

References and Notes

(1) Bizzarri, M.; Cacelli, I.; Prampolini, G.; Tani, A. *J. Phys. Chem. A* **2004**, *108*, 10336.

(2) Cacelli, I.; Prampolini, G.; Tani, A. *J. Phys. Chem. B* **2005**, *109*, 3531.

(3) Hackett, E.; Manias, E.; Giannelis, E. *Chem. Mater*. **2000**, *12*, 2161.

(4) Harmandaris, V.; Mavrantzas, V.; Theodorou, D.; Kroeger, M.; Ramirez, J.; Oettinger, H.; Vlassopoulos, D. *Macromolecules* **2003**, *36*, 1376.

(5) *Advances in the Computer Simulations of Liquid Crystals*; NATO ASI series; Pasini, P., Zannoni, C., Eds.; Kluwer: Dordrecht, 2000.

(6) *Computer Simulations of Liquid Crystals and Polymers*; NATO ASI series; Pasini, P., Zannoni, C., Zumer, S., Eds.; Kluwer: Dordrecht, 2005.

(7) Cacelli, I.; Cinacchi, G.; Prampolini, G.; Tani, A. *J. Am. Chem. Soc*. **2004**, *126*, 14278.

(8) deGennes, P.; Prost, J. *The Physics of Liquid Crystals*, 2nd ed.; Oxford University Press: Oxford, 1993.

(9) Glaser, M.; Clark, N.; Garcia, E.; Walba, D. *Spectrochim. Acta A* **1997**, *53*, 1325.

(10) Crain, J.; Komolkin, A. *Adv. Chem. Phys*. **1999**, *109*, 39.

(11) Glaser, M. A. Atomistic simulation and modeling of smectic liquid crystals in Advances in *Computer Simulations of Liquid Crystals*; NATO ASI series; Pasini, P., Zannoni, C.; Kluwer: Dordrecht, 2000.

(12) Demus, D., Goodby, J., Gray, G. W., Spiess, H. W., Vill, V., Eds.; *Handbook of Liquid Crystals* (Vol. 1, Fundamentals); Wiley-VCH: Weinheim, 1998.

(13) Yakovenko, S.; Muravski, A.; Eikelschulte, F.; Geiger, A. *Liq. Cryst*. **1998**, *24*, 657.

(14) Amovilli, C.; Cacelli, I.; Campanile, S.; Prampolini, G. *J. Chem. Phys*. **2002**, *117*, 3003.

(15) Cacelli, I.; Cinacchi, G.; Geloni, C.; Prampolini, G.; Tani, A. *Mol. Cryst. Liq. Cryst*. **2003**, *395*, 171.

(16) Cacelli, I.; Cinacchi, G.; Prampolini, G.; Tani, A. Computer Simulation of Mesogen with ab initio Interaction Potentials in *Novel Approaches to the Structure and Dynamics of Liquids. Experiments, Theories and Simulation*; Samios, J., Durov, V., Eds.; Kluwer: Dordrecht, 2004.

(17) Mansare, T.; Decrassain, R.; Gors, C.; Dolganov, V. *Mol. Cryst. Liq. Cryst*. **2002**, *382*, 97.

(18) Oweimreen, G.; Morsy, M. *Thermochim. Acta* **2000**, *346*, 37.

(19) Dong, R. *J. Chem. Phys*. **1988**, *88*, 3962.

(20) Dong, R.; Richards, G. *Chem. Phys. Lett*. **1992**, *200*, 541.

(21) Dong, R. *Phys. Rev. E* **1998**, *57*, 4316.

(22) Calucci, L.; Geppi, M. *J. Chem. Inf. Comput. Sci*. **2001**, *41*, 1006.

(23) Catalano, D.; Cifelli, M.; Geppi, M.; Veracini, C. *J. Phys. Chem. A* **2001**, *105*, 34.

(24) Wacrenier, J.; Duron, C.; Lippens, D. *Mol. Phys*. **1981**, *43*, 97.

(25) Watanabe, H.; Sato, T.; Hirose, M.; Osaki, K.; Yao, M. *Rheol. Acta* **1998**, *37*, 519.

(26) Paschen, D.; Geiger, A. MOSCITO 3.9; Department of Physical Chemistry: University of Dortmund, 2000.

(27) Berendsen, H. J. C.; Postma, J. P. M.; van Gunsteren, W. F.; Di Nola, A.; Haak, J. R. *J. Chem. Phys*. **1984**, *81*, 3684.

(28) Ryckaert, J. P.; Ciccotti, G.; Berendsen, H. J. C. *J. Comput. Phys*. **1977**, *55*, 3336.

(29) Allen, M.; Tildesley, D. *Computer Simulation of Liquids*; Clarendon: Oxford, 1987.

(30) Darden, T.; York, D.; Pedersen, L. *J. Chem. Phys*. **1993**, *98*, 10089.

(31) Essmann, U.; Perera, L.; Berkowitz, M.; Darden, A.; Lee, H.; Pedersen, L. *J. Chem. Phys*. **1995**, *103*, 8577.

(32) *Molecular Dynamics of Liquid Crystals*; NATO ASI seires; Luckhurst, G. R., Veracini, C. A.; Kluwer: Dordrecht, 1994.

(33) Steele, W. A. *J. Chem. Phys*. **1963**, *38*, 2404.

(34) Adam, C.; Clark, S. J.; Ackland, G. J.; Crain, J. *Phys. Rev. E* **1997**, *55*, 5641.

(35) Raynes, E. P. *Mol. Cryst. Liq. Cryst. Lett*. **1985**, *1*, 69.

(36) Hansen, J.; McDonals, I. R. *Theory of Simple Liquids*; Academic Press: New York, 1986.

(37) Cozzini, S.; Rull, L. F.; Ciccotti, G.; Paolini, G. V. *Physica A* **1997**, *240*, 173.

(38) Sarman, S.; Evans, D. J. *J. Chem. Phys*. **1993**, *99*, 9021.

(39) Zwanzig, R.; Ailawadi, N. *Phys. Rev*. **1969**, *182*, 280.

(40) Hanemann, T.; Haase, W.; Svodoba, I.; Fuess, H. *Liq. Cryst*. **1995**, *19*, 699.

(41) Dvinskikh, S.; Furo', I. *J. Chem. Phys*. **2001**, *115*, 1946.

(42) Jadzin, J.; Czechowsky, G. *Phys. Rev. E* **2003**, *67*, 041705.

(43) Deeg, F.; Greenfield, S.; Stankus, J.; Newell, V.; Fayer, M. *J. Chem. Phys*. **1990**, *93*, 3503.

(44) Gottke, S.; Cang, H.; Bagchi, B.; Fayer, M. *J. Chem. Phys*. **2002**, *116*, 6339.

(45) Li, J.; Wang, I.; Fayer, M. *J. Phys. Chem. B* **2005**, *109*, 6514.
(46) Jadzin, J.; Lech, R. D. T.; Czechowski, G. *J. Chem. Eng. Data* **2001**, *46*, 110.
(47) Sarman, S. *J. Chem. Phys*. **1998**, *108*, 7909.
(48) Chmielewski, A. *Mol. Cryst. Liq. Cryst*. **1986**, *132*, 339.
(49) Cui, M.; Kelly, J. *Mol. Cryst. Liq. Cryst*. **1999**, *331*, 49.
(50) Wu, S.; Wu, C. *Phys. Rev. A* **1990**, *42*, 2219.
(51) Kneppe, H.; Schneider, F.; Shaarma, N. *J. Chem. Phys*. **1982**, *77*, 3203.
(52) Zakharov, A.; Komolkin, A. V.; Maliniak, A. *Phys. Rev. E* **1999**, *59*, 6802.
(53) Kuwajima, S.; Manabe, A. *Chem. Phys. Lett*. **2000**, *332*, 104.
(54) Capar, M. I.; Cebe, E. *Chem. Phys. Lett*. **2005**, *407*, 454.
(55) Adam, C.; Ferrarini, A.; Wilson, M.; Ackland, G.; Crain, J. *Mol. Phys*. **1999**, *97*, 541.